LA-UR-14-24364
Approved for public release; distribution is unlimited.

Title: A Verification of MCNP6 FMESH Tally Capabilities

Author(s): Swift, Alicia L.
McKigney, Edward A.
Schirato, Richard C.
Temple, Brian A.
Robinson, Alex P.

Intended for: 2014 American Nuclear Society (ANS) Winter Meeting, 2014-11-09
(Anaheim, California, United States)

Issued: 2014-09-12 (rev.3)

A Verification of MCNP6 FMESH Tally Capabilities

Alicia L. Swift, Edward A. McKigney, Richard C. Schirato, Alex P. Robinson, Brian A. Temple

Los Alamos National Laboratory, Los Alamos, New Mexico, alicia.swift@lanl.gov

INTRODUCTION

MCNP6 is a Monte Carlo physics code with many capabilities, such as criticality calculations, flux-to-dose conversions, and radiography [1]. For the latter application, MCNP6 uses FMESH tallies to conduct imaging simulations. These tallies place a voxel mesh over a volume (such as a detector) and divide the total particle track length by the voxel volume to generate the particle fluence in each voxel [2]. Tallies are then plotted to form simulated images. However, because FMESH tallies do not have some of the same statistical checks as other routines in MCNP6, it is important that studies are conducted to ensure FMESH tallies are properly representing the physics and statistics of particle interactions. This work is one such verification of the MCNP6 FMESH tally capabilities and compares simulated neutron time-of-flight (TOF) data with analytic calculations and another MCNP6 tally.

DESCRIPTION OF THE ACTUAL WORK

This work serves to verify the MCNP6 FMESH capability through comparison to two types of data. FMESH tallies, binned in time, were generated on an ideal detector face for neutrons undergoing a single scatter in a graphite target. For verification, FMESH results were compared to analytic calculations of the non-relativistic TOF for elastic and inelastic single neutron scatters (TOF for the purposes of this paper is the time for a neutron to travel from its scatter location in the graphite target to the detector face). FMESH tally results were also compared to F4 tally results, an MNCP tally that calculates fluence in the same way as the FMESH tally.

MCNP6 FMESH Tally Simulations

A simple geometry was simulated with MCNP6 and was comprised of a monoenergetic (E=10.17 MeV, 100 x 10^9 particles) neutron pencil beam incident on the center of a graphite target (5 x 50 x 50 cc) (Fig. 1). The beam was located 0.25 cm from the center of the target surface, with an ideal detector (5 x 100 x 100 cc) located on the opposite side of the target. The front face of the detector was placed 100 cm from the center of the graphite target. All neutrons entering the front face of the detector were immediately killed so as to replicate 100% efficiency. An FMESH tally covered the face of the detector and consisted of 1 x 50 x 50 voxels (7 x 2 x 2 cc). The tally was set up to represent detector time binning, with bin widths of 1.0 ns. The FMESH tally only recorded neutrons that had a single scatter reaction in the target.

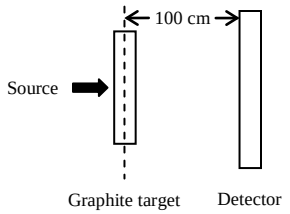

Fig. 1. Simulated geometry of a monoenergetic neutron pencil beam incident on a graphite slab target, with an ideal detector located 100 cm from the target centerline.

Analytic Calculations

Upon inspection of the FMESH tally results, a time-dependent ring structure at the detector surface was evident. The rings, three in total over the simulated time interval of 50 μs, began at the center of the detector face and grew radially as time progressed, one appearing after the other. This is because the TOF increases as the scattering angle increases due to an increased distance that must be traveled by the neutron. The radius is a result of this increased scattering angle, with larger radii being seen at later times. It should be noted that a ring is seen, instead of other shapes, because of the symmetry in the simulated geometry. The growth in time of the first of the three rings (Ring 1) is shown in Fig. 2; Rings 2 and 3 behaved similarly.

It should be noted that each ring corresponds to a particular scattering reaction, each with a different range of possible TOF for the given geometry. Ring 1 is caused by elastic scatter in the graphite target. This is because elastic scatter is the scattering reaction with the least amount of energy loss (thereby having the highest neutron velocity), and so elastic scatters arrive at the detector face first. The later arrival of the second and third rings is explained by neutrons suffering inelastic scattering collisions. This type of reaction must overcome a reaction threshold, Q, which causes the outgoing neutron velocity to be much lower than that from elastic scatter and the TOF to be much greater. The third ring has a greater Q (and therefore a larger TOF) than the second ring and is seen to arrive last.

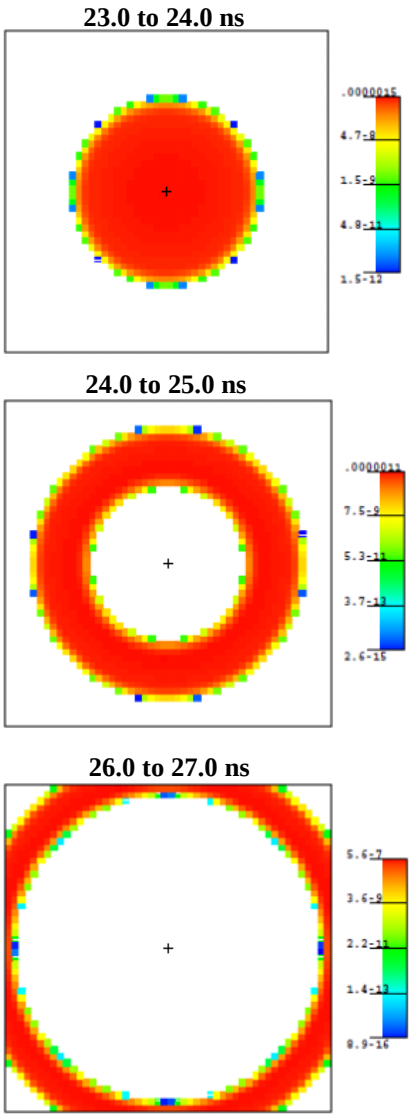

Fig. 2. Simulated time-dependent behavior of Ring 1 on the detector face. Note that that color scale varies among time bins and indicates the number of neutrons detected per source particle. Rings 2 and 3 behaved similarly.

As verification of the MCNP6 FMESH tally capability, the ring structure seen in the simulations was compared to analytic calculations of the TOF of single-scattered neutrons. Both elastic and inelastic scatter reactions were calculated using trigonometry and kinematics. Two scattering locations in the graphite target were selected as the site of the single scatter (e.g. front and back of the center of the graphite target, where 'front' is the side of the target facing the source). Three locations on the detector face were selected for TOF comparisons (Case I: center, Case II: center of the top edge, and Case III: top left corner) (Fig. 3).

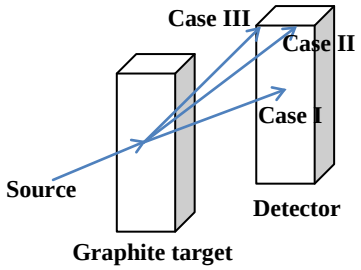

Fig. 3. Neutron undergoing a single scatter in the graphite target and traveling to three locations on the detector face selected for verification: Case I, Case II, and Case III.

Elastic Scatter Time-of-Flight

Elastic scatter reaction calculations assumed a billiard ball interaction with a stationary graphite target nucleus. As previously stated, elastic scatter reactions conserve kinetic energy, whereas other reactions lose energy to processes such as exciting the nucleus. As a result, the neutrons suffering an elastic scatter will arrive at a detector before the neutrons undergoing another interaction, seen in the simulations as Ring 1.

Calculations were conducted in two parts. The first step used trigonometry to determine the scattering distance, *d*, and angle traveled by the neutron from its target scattering location (front or back of the target) to Case I, Case II, or Case III on the face of the detector. The second step used nonrelativistic kinematic equations to calculate the velocity, *v'*, of the neutron after an elastic scatter. The TOF was then calculated with Equation 1 below if scattered from the front of the target. Equation 2 was used if the neutron scattered from the back of the target, accounting for the time of travel through the target of thickness, *h*, at the initial neutron velocity, *v*, prior to scatter.

$$TOF_{front} = \frac{d}{v'} \quad (1)$$

$$TOF_{back} = \frac{d}{v'} + \frac{h}{v} \quad (2)$$

Inelastic Scatter Time-of-Flight

Inelastic scatter is different from elastic scatter in that, instead of a billiard ball reaction, the incident neutron is absorbed by the nucleus, exciting it and forming a compound nucleus. This excited state then decays, yielding ejectiles such as a neutron. For this excitation of the nucleus to occur, the incident neutron energy must be greater than the threshold energy, which depends on the atomic structure of the target atom and the inelastic scattering level. As atomic structures become more complex, more inelastic scattering reactions are

possible. According to ENDF/B-VII.0 neutron cross-section data for graphite, there are thirteen possible inelastic scattering reactions. However, given the geometry and neutron source constraints (i.e. incident neutron energy and outgoing scattering angle), only two of these reactions are feasible: Level 1 (Q=4.44 MeV) and Level 2 (Q=7.65 MeV) inelastic scatter. TOF calculations were performed similarly to elastic scatter, using trigonometry and kinematics, while taking into account the reaction threshold energy.

MCNP6 F4 Tally Simulations

In addition to the analytic calculations, the FMESH results were also compared to those from an F4 tally. The F4 tally was selected because it, like the FMESH tally, averages neutron track length over volume to yield fluence. However, instead of finding the fluence in voxels like the FMESH tally, the F4 tally uses cells. The F4 tally also uses more rigorous statistical checks, making it useful for verification purposes.

The F4 tally was comprised of three cells of the same size as the FMESH voxels (7 x 2 x 2 cc) and in the locations specified by Case I, Case II, and Case III (Fig. 4). As with the FMESH tally, the F4 tally immediately killed neutrons entering the cells, thereby simulating an ideal detector. Time bins were also the same as those used in the FMESH tally. Time bins when counts first appeared in the cells were noted and compared to first counts in the FMESH time bins The F4 tally simulated 100 x 10^9 particles to remain consistent with the FMESH tally.

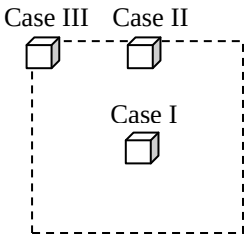

Fig. 4. Illustration of the three cells (solid line) used for the F4 tally. These cells had the same size and location as the FMESH voxels of interest. The detector face is shown for reference (dashed line).

RESULTS

FMESH Simulations vs. Analytic Calculations

As can be seen in Table 1, the elastic scatter TOF results match almost exactly with the FMESH simulated data (i.e. the times that Ring 1 reached Case I, Case II and Case III on the detector face). For all results presented, percent error was calculated if the data fell outside of the time bin, and was calculated for the nearest time bin endpoint. The sign of the error indicates whether the FMESH time bin is above (+) or below (-) the analytic TOF. For elastic scatter, the data was seen to match exactly.

Table I. Single elastic scatter analytic TOF vs. Ring 1 simulated FMESH data

	Location	Analytic TOF (ns)	FMESH TOF (ns)	Percent Error (%)
Front of target scatter	Case I	23.0	23.0 to 24.0	–
	Case II	25.9	25.0 to 26.0	–
	Case III	28.5	28.0 to 29.0	–
Back of target scatter	Case I	23.0	23.0 to 24.0	–
	Case II	25.9	25.0 to 26.0	–
	Case III	28.6	28.0 to 29.0	–

Level 1 and Level 2 inelastic scatter results can be seen in Table II and Table III below, which correspond respectively to Ring 2 and Ring 3. The inelastic scatter results were seen to overall match well with the FMESH tally data. The results also make logical sense; Level 1 inelastic scatter has a lower reaction threshold than Level 2 inelastic scatter, so outgoing neutrons from this reaction should travel faster and reach the detector face before Level 2 inelastic scatter. This is what was seen to happen with Ring 2 and Ring 3. Again, percent error was calculated if the analytic time fell outside of the FMESH time bin.

Table II. Level 1 single inelastic scatter analytic TOF vs. Ring 2 simulated FMESH data

	Location	Analytic TOF (ns)	FMESH TOF (ns)	Percent Error (%)
Front of target scatter	Case I	30.8	30.0 to 31.0	–
	Case II	34.7	34.0 to 35.0	–
	Case III	38.3	37.0 to 38.0	0.8
Back of target scatter	Case I	30.6	30.0 to 31.0	–
	Case II	34.6	34.0 to 35.0	–
	Case III	38.3	37.0 to 38.0	0.8

Table III. Level 2 single inelastic scatter analytic TOF vs. Ring 3 simulated FMESH data

	Location	Analytic TOF (ns)	FMESH TOF (ns)	Percent Error (%)
Front of target scatter	Case I	48.6	47.0 to 48.0	1.2
	Case II	55.3	53.0 to 54.0	2.4
	Case III	61.3	58.0 to 59.0	3.8
Back of target scatter	Case I	47.8	47.0 to 48.0	–
	Case II	54.7	53.0 to 54.0	1.3
	Case III	60.9	58.0 to 59.0	3.1

FMESH Simulations vs. F4 Simulations

FMESH results for the TOF of the rings matched exactly with F4 results (Table IV). This indicates FMESH results are in line with other tallies that have more rigorous statistical checks.

Table IV. Comparison of F4 and FMESH simulated results

	Location	F4 TOF (ns)	FMESH TOF (ns)	Percent Error
Ring 1	Case I	23.0 to 24.0	23.0 to 24.0	–
	Case II	25.0 to 26.0	25.0 to 26.0	–
	Case III	28.0 to 29.0	28.0 to 29.0	–
Ring 2	Case I	30.0 to 31.0	30.0 to 31.0	–
	Case II	34.0 to 35.0	34.0 to 35.0	–
	Case III	37.0 to 38.0	37.0 to 38.0	–
Ring 3	Case I	47.0 to 48.0	47.0 to 48.0	–
	Case II	53.0 to 54.0	53.0 to 54.0	–
	Case III	58.0 to 59.0	58.0 to 59.0	–

Discussion of Error

In general, error between the analytic TOF calculations (both elastic and inelastic) and simulated FMESH results can be attributed to the method for deciding when a ring first reached a location (e.g. Case I, II, or III) on the detector face. FMESH tallies were plotted with MCPLOT, MCNP's plotting tool, to form simulated images, which were then visually analyzed to determine when the ring in question reached the three locations of interest. This has the potential to be less accurate than a calculation. Another potential source of discrepancy between the analytic and FMESH results could be the analytic calculations themselves. For simplicity of calculation, reactions were assumed to be non-relativistic and to only occur at two locations of scatter in the graphite target. In reality, scatter would occur throughout the graphite target, which adds a blurring term to the neutron ring seen at the detector face.

FMESH and F4 tally relative error, while generally low, increased in two instances. First, it was difficult to get particles to scatter to Case III, resulting in a lower count rate and a higher relative error than Case I or II (see Table II and III). For example, the average FMESH counts per source particle were $\sim 10^{-7}$ for Ring 1 and 2, compared to $\sim 10^{-12}$ for Ring 3. Average MCNP-generated relative error was 0.08%, 0.17%, and 24.5%, respectively. Second, counts predictably decreased directly with the reaction cross section (where $\sigma_{el} > \sigma_{inel,L1} > \sigma_{inel,L2}$), causing an increase in MCNP relative error. For both tallies, these two factors led to the highest error for Ring 3, Case III (57.4% and 49.2%, respectively). In the future, this can be addressed with variance reduction and more particles.

CONCLUSIONS AND FUTURE WORK

Given how well the FMESH tally results agree with the analytic results and the F4 tally, it is believed that, for simple geometries, MCNP6 FMESH tallies represent the physics of neutron scattering very well. Variance reduction and an increased number of simulated particles should reduce error in future work. Additional verification efforts should be expanded to include simulations with smaller time bins, more complicated geometries, relativistic TOF equations, and other particle interactions.

NOMENCLATURE

Q = reaction threshold energy for inelastic scatter
d = distance traveled by neutron after scatter
h = distance traveled through target prior to scatter
v' = neutron velocity after scatter
v = neutron velocity prior to scatter
TOF = time-of-flight for a scattered neutron

REFERENCES

1. John T. Goorley et al., "MCNP6 User's Manual: Version 1.0," Los Alamos Technical Report (LA-CP-13-00634), May 2013.
2. Brian Temple, "Differences between the TALLYX and fmesh cell tagging capabilities," Los Alamos Technical Report (LA-UR-04-8244), 12 November 2004.